Three-Color Alternating-Laser Excitation of Single Molecules: Monitoring Multiple Interactions and Distances

Nam Ki Lee,* Achillefs N. Kapanidis,†‡ Hye Ran Koh,* You Korlann,† Sam On Ho,† Younggyu Kim,† Natalie Gassman,† Seong Keun Kim,* and Shimon Weiss†

*School of Chemistry, Seoul National University, Seoul, Korea; †Department of Chemistry and Biochemistry, and Department of Physiology, University of California, Los Angeles, California; and ‡Clarendon Laboratory, Department of Physics, and IRC in Bionanotechnology, University of Oxford, Oxford, United Kingdom

ABSTRACT We introduce three-color alternating-laser excitation (3c-ALEX), a fluorescence resonance energy transfer (FRET) method that measures up to three intramolecular distances and complex interaction stoichiometries of single molecules in solution. This tool extends substantially the capabilities of two-color ALEX, which employs two alternating lasers to study molecular interactions (through probe stoichiometry *S*) and intramolecular distances (through FRET efficiency *E*), and sorts fluorescent molecules in multi-dimensional probe-stoichiometry and FRET-efficiency histograms. Probe-stoichiometry histograms allowed analytical sorting, identification, and selection of diffusing species; selected molecules were subsequently represented in FRET-efficiency histograms, generating up to three intramolecular distances. Using triply labeled DNAs, we established that 3c-ALEX enables 1), FRET-independent analysis of three-component interactions; 2), observation and sorting of singly, doubly, and triply labeled molecules simultaneously present in solution; 3), measurements of three intramolecular distances within single molecules from a single measurement; and 4), dissection of conformational heterogeneity with improved resolution compared to conventional single-molecule FRET. We also used 3c-ALEX to study large biomolecules such as RNA polymerase-DNA transcription complexes, and monitor the downstream translocation of RNA polymerase on DNA from two perspectives within the complex. This study paves the way for advanced single-molecule analysis of complex mixtures and biomolecular machinery.

INTRODUCTION

Elucidation of biological mechanisms requires understanding of the processes involved in the assembly (and disassembly) of biomachinery, as well as of the conformational changes that enable its function. Assembly and disassembly processes add components to or remove them from biomachinery, changing its molecular stoichiometry, whereas conformational changes reposition molecular parts, changing the spatial relations among modules of a biomachine. Such changes have been studied using fluorescence resonance energy transfer (FRET), both at the ensemble (1–3) and single-molecule levels (4–6). Most FRET experiments employ a pair of complementary fluorescent probes, a donor and an acceptor; when the donor and acceptor probes are $<$8–10 nm apart, the measured FRET efficiency can report a single interprobe distance and a bimolecular interaction (1,6).

Recently, several groups introduced ensemble-based three-color FRET (3c-FRET) approaches, which use molecules labeled with three probes, each having a distinct emission spectrum (Fig. 1, *A* and *B*; *B* (blue probe), *G* (green probe), and *R* (red probe)) to monitor three-molecule interactions and up to three interprobe distances (7–18). At the single-molecule level, often the only level for handling extensive compositional or conformational heterogeneity, 3c-FRET has also been realized for surface-immobilized (19) and diffusing molecules (20,21), establishing the potential of 3c-FRET for probing complex dynamics of biomolecules.

However, the existing single-molecule 3c-FRET methods are not general, as they depend heavily on the presence of substantial FRET between all probes to report on interactions and distances. Thus, the heavy dependence on FRET does not permit the study of trimolecular interactions when the probes are spaced by $>7-10$ nm in the resulting trimolecular complex; in this case, triply labeled species are essentially indistinguishable from either singly labeled (e.g., *B* only (Fig. 1 *B*)) or doubly labeled species (e.g., *B*-*G*, *B*-*R* (Fig. 1 *B*)) present in the sample either as free interactants or as a result of inactive states of probes (22). Moreover, no existing method can detect species present in the interaction equilibrium but not appreciably excited by the single-laser excitation used in these methods (such as species *G*-*R*, *G*-only, and *R*-only (Fig. 1 *B*)). Finally, in studies of multiple interprobe distances, the existing methods cannot easily measure accurate FRET from single molecules, especially without auxiliary experiments that measure FRET between individual pairs. These limitations cannot be addressed by ensemble-type 3c-FRET (12,13).

Here, we introduce three-color alternating-laser excitation (3c-ALEX), a general method that overcomes the above limitations by implementing alternating-laser excitation (Fig. 1 *C*) of single molecules labeled with up to three fluorescent probes. The new method is a substantial extension of two-color

Submitted July 13, 2006, and accepted for publication September 11, 2006.

Address reprint requests to Seong Keun Kim, School of Chemistry, Seoul National University, Seoul 151-747, Korea. Tel.: 82-2-880-6659; Fax: 82-2-889-5719; E-mail: seongkim@snu.ac.kr; or to Shimon Weiss, Dept. of Chemistry and Biochemistry, University of California, Los Angeles, 607 Charles E. Young Dr., E. Los Angeles, CA 90095. Tel.: 310-794-0093; Fax: 310-267-4672; E-mail: sweiss@chem.ucla.edu.

0006-3495/07/01/303/10 $2.00

doi: 10.1529/biophysj.106.093211

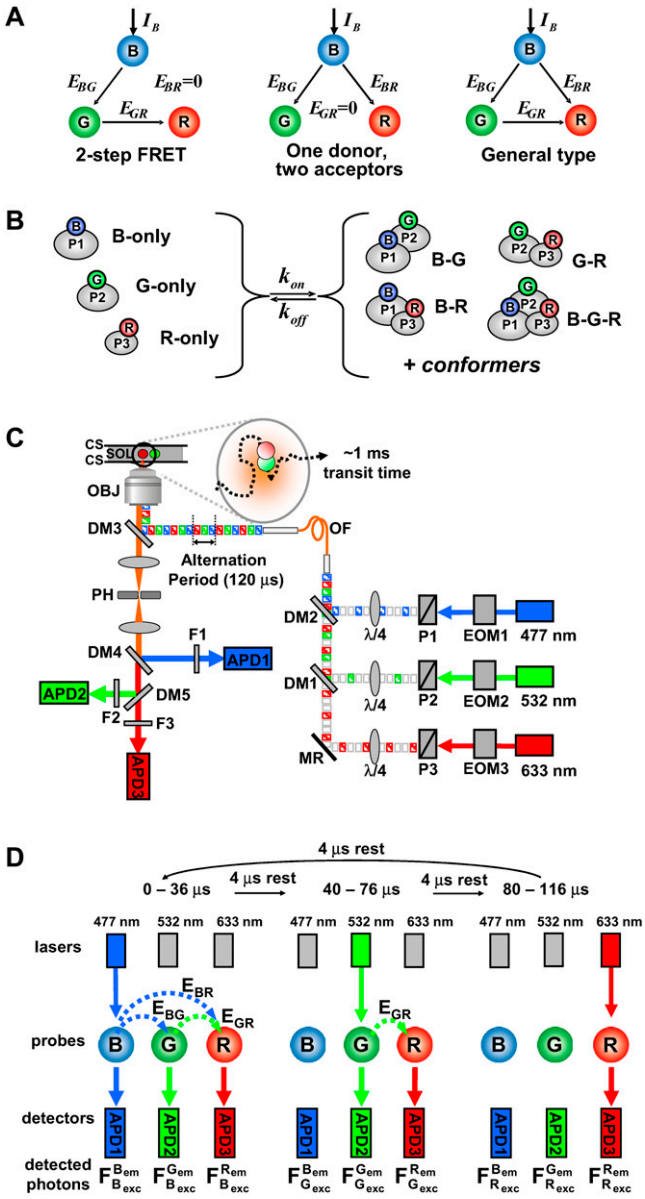

FIGURE 1 Three-color ALEX (3c-ALEX) spectroscopy: concept and instrumentation. (*A*) The excited-state energy of *B* is transferred to *G* and/or to *R*, and that of *G* to *R*. FRET efficiencies E_{BG}, E_{GR}, and E_{BR} provide up to three interprobe distances. I_B, excitation of probe *B*. (*A*, *left*) Two-step FRET ($E_{BR} = 0$); (*A*, *middle*) two parallel one-step FRET processes ($E_{GR} = 0$); (*A*, *right*) general case with all possible FRET processes. (*B*) Three-component interactions may produce stoichiometry-based heterogeneity (due to the presence of singly, doubly, and triply labeled species), or conformational heterogeneity (due to various conformations of a species). (*C*) The 3c-ALEX microscope. λ/4, quarter-wave plate; *APD*, avalanche photodiode; *DM*, dichroic mirror; *EOM*, electro-optical modulator; *F*, filter; *MR*, mirror; *OBJ*, objective; *OF*, optical fiber; *PH*, pinhole; *P*, polarizer. EOMs combined with polarizers lead to alternating-laser excitation. Fluorescent emissions are detected by APDs (APD1 for *B*, APD2 for *G*, and APD3 for *R*). (*D*) Photon emission streams in 3c-ALEX. The 477-nm laser excites *B* in the 0–36 μs domain, generating photon counts $F^{B_{em}}_{B_{exc}}$, $F^{G_{em}}_{B_{exc}}$, $F^{R_{em}}_{B_{exc}}$ (via FRET (E_{BG}, E_{GR}, and E_{BR})); the 532-nm laser excites *G* in the 40–76 μs domain, generating $F^{G_{em}}_{G_{exc}}$, $F^{R_{em}}_{G_{exc}}$ via E_{GR}; and the 633-nm laser excites *R* in the 80–116 μs domain, generating $F^{R_{em}}_{R_{exc}}$. Ratios based on these six photon counts report FRET efficiencies *E* and probe stoichiometries *S*.

(2c)-ALEX (23–25), which employs two alternating lasers to study molecular interactions (through probe stoichiometry ratio *S*) and intramolecular distances (through FRET efficiency *E*). In 2c-ALEX, molecules are sorted in a two-dimensional histogram of *S* and *E*, whereas 3c-ALEX sorts molecules in three-dimensional stoichiometry and three-dimensional FRET histograms. The stoichiometry histograms allowed identification and selection of molecules according to probe-stoichiometry; selected molecules were subsequently represented in FRET-efficiency histograms, where three intermolecular distances were observed. Using triply labeled DNAs (Fig. 2), we demonstrated that 3c-ALEX allows 1), FRET-independent analysis of three-component interactions; 2), observation and sorting of singly, doubly, and triply labeled molecules present in the same solution; 3), measurements of three intramolecular distances within a species even in the absence of substantial FRET among the probes; and 4), dissection of conformational heterogeneity with improved resolution compared to conventional single-molecule FRET (hereafter, 2c-FRET). We used 3c-ALEX to study large biomolecules such as complexes of RNA polymerase (RNAP) with DNA, and to monitor RNAP translocation on DNA from two perspectives within the complex. Single-molecule analysis of complex mixtures and biomolecular machinery should be greatly improved by using 3c-ALEX.

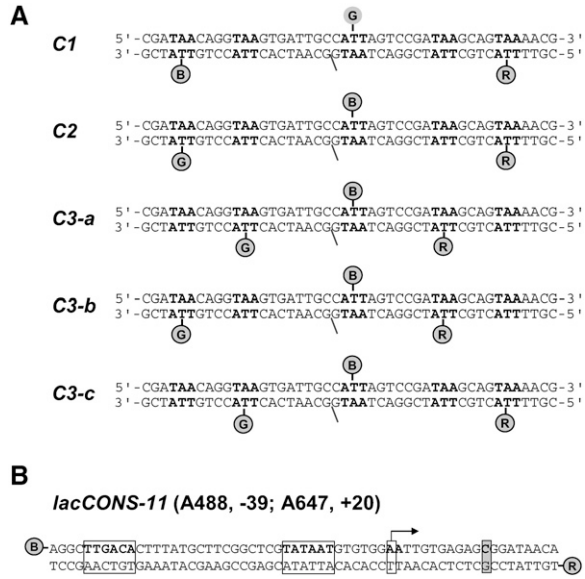

FIGURE 2 DNA fragments used for 3c-ALEX. (*A*) *C1*, *C2*, and *C3-a* are designed to represent three types of 3c-FRET (Fig. 1 *A*). Fragments *C3-b* and *C3-c* are designed to test the ability of 3c-ALEX to monitor conformational changes. (*B*) DNA fragment used in the analysis of RNAP-DNA complex. Use of this promoter-DNA fragment derived form the *lac* promoter, a stable transcription elongation complex halted after synthesis of 12 nt of RNA can be generated (see Materials and Methods). *Black boxes*, transcription start site (*arrow*), promoter −10 element and promoter −35 element; *gray box*, halt site.

MATERIALS AND METHODS

Principle of 3c-ALEX

In 2c-ALEX, a donor-excitation laser measures FRET efficiency E and probes the donor presence in a molecule, while an acceptor-excitation laser simultaneously directly probes the acceptor presence (23). The ratio of the photon counts due to two individual laser excitations reports on probe stoichiometry S. The two-dimensional E-S histogram allows fluorescence-aided molecule sorting. Similarly, 3c-ALEX can measure E and S simultaneously for a three-probe system (B-G-R, where probe B can serve as a donor to probes G and R, and where probe G can serve as a donor to probe R (Fig. 1 *A*)) from single diffusing molecules, employing three lasers and three detectors (Fig. 1 *C*). Each laser excites primarily one of the three probes, and the lasers are modulated faster (120 μs) than the diffusion time of a molecule through the observation volume (~1 ms). The fluorescence emissions of the three probes are subsequently detected using three detectors.

The first laser, at 477 nm, excites primarily probe B for the time domain of 0–36 μs within a 120-μs modulation period (Fig. 1 *D*, *left*). The excited-state energy of B may be transferred to G and R via FRET (Fig. 1 *A*), generating photon counts $F^{B_{em}}_{B_{exc}}$, $F^{G_{em}}_{B_{exc}}$, and $F^{R_{em}}_{B_{exc}}$ (which denote cross-talk-corrected photon counts from a single fluorescent molecule excited by a 477-nm laser and detected by B-, G-, and R-detectors, respectively; for details see Supplementary Material, Theory of 3c-ALEX and Fig. S1). The three photon counts are used for calculating the following FRET-related ratios:

$$E^*_{BG} = F^{G_{em}}_{B_{exc}}/(F^{B_{em}}_{B_{exc}} + F^{G_{em}}_{B_{exc}}); \quad (1)$$

and

$$E^*_{BR} = F^{R_{em}}_{B_{exc}}/(F^{B_{em}}_{B_{exc}} + F^{R_{em}}_{B_{exc}}), \quad (2)$$

where E^*_{XY} is a proximity ratio (an approximation of FRET efficiency E_{XY} (22)). However, proximity ratios E^*_{BG} and E^*_{BR} (also encountered in single-laser 3c-FRET (20)) cannot determine all possible FRET efficiencies among the three probes within a single molecule. To recover the complete set of FRET efficiencies in the case of single-excitation 3c-FRET, an additional measurement on a doubly labeled species is required (20); this is difficult when simultaneous monitoring of three distances within a single molecule is sought, or when analysis of multi-conformer mixtures is performed. In 3c-ALEX, however, the presence of a second laser allows determination of all three FRET efficiencies (and corresponding distances) from single molecules.

The second laser, at 532 nm, excites primarily probe G for the time domain of 40–76 μs (Fig. 1 *D*, *middle*). The excited-state energy of G may be transferred to R via FRET, generating two nonzero photon counts, $F^{G_{em}}_{G_{exc}}$ and $F^{R_{em}}_{G_{exc}}$; the two photon counts define proximity ratio E^*_{GR}, the ratio not available in single-excitation 3c-FRET:

$$E^*_{GR} = F^{R_{em}}_{G_{exc}}/(F^{G_{em}}_{G_{exc}} + F^{R_{em}}_{G_{exc}}). \quad (3)$$

The three proximity ratios yield three corrected FRET efficiencies (E_{BG}, E_{GR} and E_{BR}; see Supplementary Material, Theory of 3c-ALEX), which directly report on three distances R_{XY}, since

$$R_{XY} = R_{0,XY}[(1/E_{XY}) - 1]^{1/6}, \quad (4)$$

where $R_{0,XY}$ is the Förster radius of the XY probe pair (3).

As in 2c-ALEX (23), 3c-ALEX can measure the probe stoichiometries of the species formed by a three-component, three-probe system independent of FRET. Since photon counts $F^{B_{em}}_{B_{exc}}$, $F^{G_{em}}_{B_{exc}}$, and $F^{R_{em}}_{B_{exc}}$ (Fig. 1 *D*) are generated by exciting probe B by the 477-nm laser, their sum, $F_{B_{exc}}$ ($F^{B_{em}}_{B_{exc}}+F^{G_{em}}_{B_{exc}}+F^{R_{em}}_{B_{exc}}$), reports on the presence of probe B in a molecule. If a molecule contains probe B, $F_{B_{exc}}$ is significant, whereas if the molecule is devoid of B, $F_{B_{exc}}$ is negligible. Likewise, the sum of 532-nm–induced photon counts, $F_{G_{exc}}$ ($F^{G_{em}}_{G_{exc}}+F^{R_{em}}_{G_{exc}}$), reports on the presence of probe G in a molecule; and the 633-nm-induced photon count $F_{R_{exc}}$ ($F^{R_{em}}_{R_{exc}}$, collected during the time domain of 80–116 μs (Fig. 1 *D*)) reports on the presence of probe R in a molecule. Using photon counts $F_{B_{exc}}$, $F_{G_{exc}}$, and $F_{R_{exc}}$, we define:

$$S_{BG} = F_{B_{exc}}/(F_{B_{exc}} + F_{G_{exc}}), \quad (5)$$

$$S_{GR} = F_{G_{exc}}/(F_{G_{exc}} + F_{R_{exc}}), \quad (6)$$

and

$$S_{BR} = F_{B_{exc}}/(F_{B_{exc}} + F_{R_{exc}}), \quad (7)$$

where S_{XY} denotes the probe stoichiometry specific to probes X and Y. Since each species generated by three-component interactions (B-only, G-only, R-only, B-G, B-R, G-R, and B-G-R (Fig. 1 *B*)) has a distinct set of probe stoichiometries (S_{BG}, S_{GR}, andS_{BR} (Fig. 3 *A*, Table)), this set can be used to sort, identify, and select molecules belonging to each species. To sort molecules based on probe stoichiometry, we devised a three-dimensional stoichiometry histogram (hereafter, S histogram (Fig. 3)). We use a similar three-dimensional proximity-ratio histogram to display the three proximity ratios (Eqs. 1–3) that characterize each diffusing molecule (Fig. 4); we refer to this histogram as the ''E* histogram''.

DNA preparation

To verify that 3c-ALEX is applicable to all 3c-FRET cases (Fig. 1 *A*), we prepared three double-stranded DNA fragments (*C1*, *C2*, and *C3-a* (Fig. 2 *A*)), which represent all three 3c-FRET cases (12). To test the ability of 3c-ALEX to measure distances, we prepared DNA fragments *C3-b* and *C3-c* which have a different set of intramolecular distances compared to *C3-a*. The three probes used were Alexa488 (probe B), carboxytetramethylrhodamine (TMR, probe G), and Alexa647 (probe R) (all from Molecular Probes, Eugene, OR) (23). For single-molecule measurements, the final DNA concentration was 50−75 pM in SM buffer (10 mM HEPES-NaOH pH 7, 500 mM NaCl, 100 μg/ml BSA, 1 mM mercaptoethylamine, and 5% glycerol). The R_o values for the B-G, G-R, and B-R pairs were 62 Å, 62 or 66 Å, and 56 Å, respectively (Supplementary Material, Ensemble measurement).

Preparation of transcription complexes

RNAP labeled at position 496 of σ^{70} was prepared using minor modifications of published protocols (26). Plasmid pGEMD496C was used for overexpression of a σ^{70} derivative with a single reactive Cys at position 496; the σ^{70} derivative was purified as described (27), but using an anion-exchange Mono Q column (Amersham Pharmacia Biotech, Piscataway, NJ) instead of DE52 resin. RNAP labeling was performed by reacting Cys-496 with Cy3B-maleimide (probe G), followed by purification on a gel-filtration column (Y. Kim and S. Weiss, unpublished), followed by reconstitution of RNAP holoenzyme by incubating Cy3B-labeled σ^{70} with RNAP core (Epicentre, Madison, WI) (26).

The DNA used for studying transcription complexes was derived from positions −39 to +20 of a lacCONS sequence (28), and was prepared as described (26), but using Alexa488- and Alexa647-labeled PCR primers (Fig. 2 *B*). RNAP-DNA complexes were prepared and analyzed as described (29), except that elongation complex $RD_{e,12}$ was formed by adding 100 μM NTPs and 500 μM 3-OMe-CTP to RP_o.

Single-molecule data acquisition and analysis

A 2c-ALEX single-molecule fluorescence microscope (23) was modified for 3c-ALEX (Fig. 1 *C*). Three laser excitation sources of 477-nm light from Ar^+ laser (35-LAP-321, Melles-Griot, Carlsbad, CA), 532-nm light from solid-state green laser (DPGL-20P, World Star Tech, Toronto, Canada), and 633-nm light from HeNe laser (25-LHP-925, Melles-Griot) were alternated using a combination of polarizers with electrooptical modulators (EOMs) (Conoptics, Danbury, CT) (23). The extinction ratios (ratios

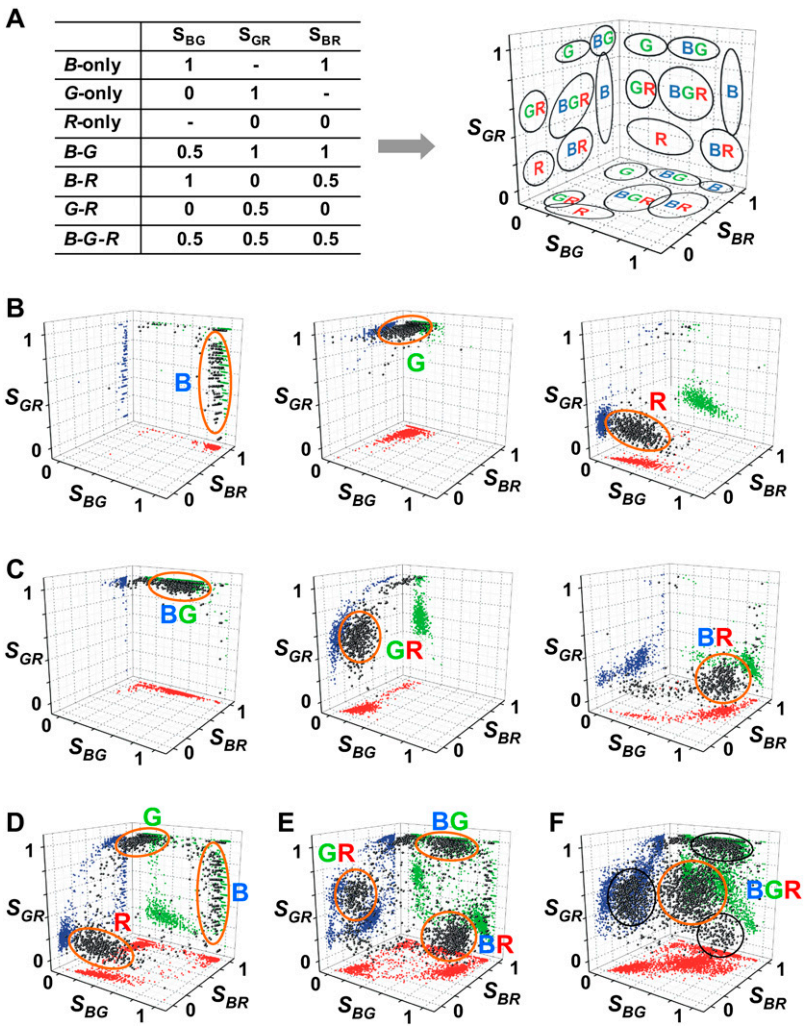

	S_{BG}	S_{GR}	S_{BR}
B-only	1	-	1
G-only	0	1	-
R-only	-	0	0
B-G	0.5	1	1
B-R	1	0	0.5
G-R	0	0.5	0
B-G-R	0.5	0.5	0.5

FIGURE 3 Molecule sorting based on probe stoichiometry *S* histograms. (*A*, *left*) Table for stoichiometry *S* of singly, doubly, and triply labeled species generated by three-component interactions (Fig. 1 *B*). (*A*, *right*) the predicted locations of each species in the projections of the three-dimensional *S* histogram, based on the Table. (*B*) *S* histograms for *B*-only, *G*-only, and *R*-only. Each species appears as a cluster of molecules. Black dots represent molecules in a three-dimensional histogram; red, green, and blue dots represent projections of the three-dimensional histogram on to S_{BG}-S_{BR}, S_{BG}-S_{GR}, and S_{BR}-S_{GR} planes, respectively. (*C*) *S* histograms for *B-G*, *G-R*, and *B-R*. The molecules of doubly labeled species are in orange ovals; trace amounts of singly labeled species also appear. (*D*) *S* histograms for 1:1:1 mixture of *B*-only, *G*-only, and *R*-only. The molecules of each species cluster at different locations of the histogram; these locations match the ones in panel *B*. (*E*) *S* histograms for 1:1:1 mixture of three doubly labeled species (*B-G*, *G-R*, and *B-R*). The molecules of each species cluster at different locations of the histogram; these locations match the ones in panel *C*. (*F*) *S* histograms of triply labeled species (*B-G-R*). The cluster at the center of the histogram (*orange ovals*) corresponds to *B-G-R*. Black ovals surround clusters corresponding to the doubly labeled species selected for FRET analysis in Fig. 4 *A*. Singly, doubly, and triply labeled species of *C1* DNA fragment (Fig. 2 *A*) were used.

of laser intensities when a laser is on or off) were typically >200:1 for each laser. The excitation beams were circularly polarized using λ/4 waveplates, coupled through two dichroic mirrors (DM1 and DM2; 560DRLP and 505DRLP; Omega Optical, Brattleboro, VT), and then spatially filtered through a single-mode fiber (460HP, Thorlabs, Newton, NJ). The coupled lights from the fiber were collimated, directed to an IX71 inverted microscope (Olympus, Tokyo, Japan), reflected on a triple-laser beamsplitter (DM3; Z488-533-633RPC, Chroma, Rockingham, VT), and focused 20 μm from the bottom coverslip through a water-immersion objective (60×, 1.2 NA, UPLAPO, Olympus). Fluorescence was collected through the objective and DM3, focused in a 100-μm pinhole, and refocused using a biconvex lens onto silicon avalanche photodiode detectors (APD) (SPCM AQR-14, EG&G, Perkin Elmer, Wellesley, MA) that were connected to a counting board (PCI-6602, National Instruments, Austin, TX). After the biconvex lens fluorescence was separated into three streams by two beamsplitters (DM4 and DM5; 560DRLP and 660DRLP, Omega Optical) and filtered in front of each APD (for Alexa 488, F1, HQ510/30; for TMR, F2, HQ600/40; for Alexa 647, F3, HQ665LP; from Chroma, McHenry, IL). The excitation intensities measured before DM3 were 60–70 μW for 477 nm, 90–120 μW for 532 nm, and 24 μW for 633 nm in alternating mode. This set of filters, beamsplitters, and excitation wavelengths reduced cross talks and background noise efficiently; the contributions of cross talks (summarized in Supplementary Material, Table S1) were <20% of main signals, and the background noises, measured using SM buffer and subtracted for data analysis, were <0.7 kHz for each detection channel. Data analysis was performed using LabVIEW (National Instruments) (24). From the 600-μs-binned photon time traces, we selected molecules using a start/stop criterion on the sum of all photon counts (for time traces, see Supplementary Material, Fig. S2). Each molecule was assigned with nine photon counts $F^{Y_{em}}_{X_{exc}}$; six photon counts (in fact, three photon counts of $F^{B_{em}}_{G_{exc}}$, $F^{B_{em}}_{R_{exc}}$, and $F^{G_{em}}_{R_{exc}}$ are zero) were used for calculating probe stoichiometries (Eqs. 5–7) and proximity ratios (Eqs. 1–3). After molecular identification, we 1), plotted *S* histograms; 2), graphically selected species of interest; 3), plotted *E** histograms for selected species and fitted them to Gaussian functions to recover mean E^*_{XY}; 4), calculated three FRET efficiencies E_{XY}; and 5), determined three distances (Eq. 4).

RESULTS AND DISCUSSION

Sorting and counting molecules using 3c-ALEX

To test whether 3c-ALEX can sort and count molecules with different probe stoichiometry, we analyzed solutions containing singly, doubly, and triply labeled DNA species, respectively, using the *C1* DNA fragment in Fig. 2 *A*.

We first examined three singly labeled species (*B*-only, *G*-only, and *R*-only), and plotted the *S* histogram for each

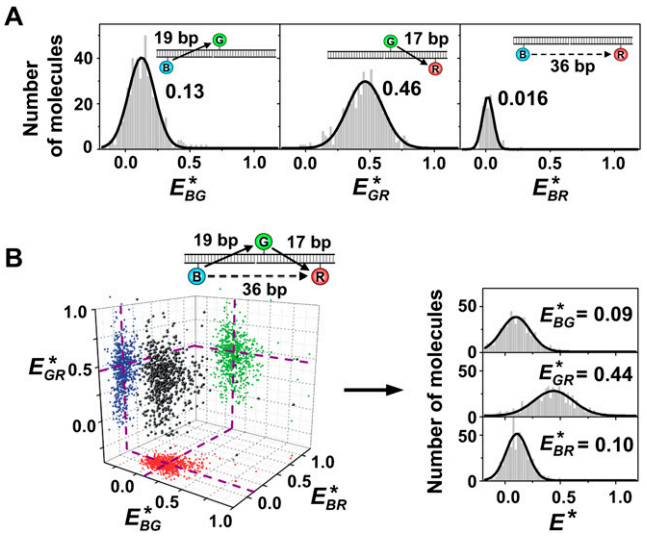

FIGURE 4 Measuring distances within triply labeled and doubly labeled species in the same solution. The reported E^* values represent the means of the fitted Gaussian distributions. (*A*) One-dimesional E^* histograms for *B-G*, *G-R*, and *B-R* species (selected as described in Fig. 3 *F*). (*B*, *left*) Three-dimensional E^* histograms for triply labeled species, *B-G-R* (selected as described in Fig. 3 *F*). (*B*, *right*) One-dimensional E^* histograms obtained after collapsing the three-dimensional histogram on each E^* axis.

species in Fig. 3 *B*. In *S* histograms, each species appeared as a cluster of points in three-dimensional space; the location of each cluster agreed well with theoretical predictions (Fig. 3 *A*). To test whether 3c-ALEX can sort and count each singly labeled species in a mixture, we examined an equimolar mixture of all three species. The three species clustered at different locations of the *S* histogram (Fig. 3 *D*); the locations matched the locations seen for pure singly labeled species (Fig. 3 *B*). To examine whether 3c-ALEX can quantify the relative abundance of each species in the mixture, we graphically selected and counted molecules for each sorted singly labeled species (Fig. 3 *D*, *ovals*). We counted 404, 452, and 462 molecules of *B*-only, *G*-only, and *R*-only species, respectively, in agreement with the equimolar mixing ratio.

Second, we examined three doubly labeled species (*B-G*, *G-R*, and *B-R*), and plotted *S* histograms for each species (Fig. 3 *C*). Again, each species appeared as a cluster of points at the predicted locations (with traces of singly labeled species due to incomplete labeling and inactive states of probes (22)). To test whether 3c-ALEX can sort and count each doubly labeled species in a mixture, we again examined an equimolar mixture of the three doubly labeled species (Fig. 3 *E*) and obtained clusters matching the ones seen for pure doubly labeled species (Fig. 3 *C*). The molecular count for the *B-G*, *G-R*, and *B-R* species was 460, 386, and 445, respectively, in good agreement with the equimolar mixing ratio.

Third, we studied a mixture containing triply labeled species *B-G-R* (Fig. 3 *F*). A comparison of Fig. 3 *F* with Fig. 3 *E* (in which all fluorescent species except *B-G-R* are present) reveals a new species at the center of the histogram in Fig. 3 *F*. The new species corresponds to *B-G-R*, for which all three probe stoichiometries are ~0.5 (Fig. 3 *A*). Since the triply labeled species is clearly isolated from singly and doubly labeled species in the *S* histogram, the triply labeled species can be easily identified and selected for further analysis.

Our results establish that 3c-ALEX permits sensitive detection, sorting, identification, and molecular counting of singly, doubly, and triply labeled species in complex mixtures. This ability renders 3c-ALEX ideal for extracting equilibrium and kinetic constants for multi-component interactions (9,10,23).

To determine whether 3c-ALEX can sort and identify molecules independent of FRET, we studied four additional DNA constructs of Fig. 2 *A* with identical probe stoichiometry but substantially different interprobe distances. The *S* histograms for all DNA constructs are essentially identical to those of *C1* (data not shown); triply labeled species cluster, as in Fig. 3 *F*. Our results establish that 3c-ALEX can sort species independent of FRET, eliminating the main shortcomings of the existing 3c-FRET methods in studying three-component interactions (9).

3c-ALEX can measure multiple distances using a single solution

Since 3c-ALEX can sort, identify, and select molecules with different probe stoichiometry for further analysis, it can be used to measure up to three distances within triply labeled molecules, and one distance within doubly labeled molecules, even when all species are in the same solution. To explore this possibility, we measured intramolecular distances for the doubly and triply labeled species sorted in Fig. 3 *F* by selecting each species and examining their E^* histograms.

All three doubly labeled species are presented in one-dimensional E^* histograms (Fig. 4 *A*). The distribution for each species is described well by a single Gaussian function, with mean values in agreement with the positions of the probes on the DNA used; E^*_{BG} is low (0.13 for 19-base-pair (bp) separation), E^*_{GR} is intermediate (0.46 for 17-bp separation), and E^*_{BR} is ~0 (0.02 for 36-bp separation).

The triply labeled species is presented in a three-dimensional E^* histogram that allows simultaneous visualization of three proximity ratios (Fig. 4 *B*, *left*); here, only a single species is observed. Mean values of 0.09, 0.44, and 0.10 for E^*_{BG}, E^*_{GR}, and E^*_{BR}, respectively, were determined from three one-dimensional E^* histograms (Fig. 4 *B*, *right*). These values agree with the positions of the probes on the DNA, as well as with those measured from doubly labeled species (Fig. 4 *A*). The small differences are due to additional FRET processes in the triply labeled species: E^*_{BG} decreases by 0.04, due to the $G \rightarrow R$ FRET, E^*_{GR} is essentially invariant (since it is independent of the presence of *B*) and E^*_{BR} increases due to the $B \rightarrow G \rightarrow R$ FRET. Our results establish that 3c-ALEX can measure multiple distances from multiple

species in a single measurement. This feature can be useful in homogeneous assays of ligand-induced conformational changes in a solution containing both a singly labeled ligand (e.g., *B*-labeled ligand) and a doubly labeled macromolecule (e.g., *G-R*-labeled macromolecule) (10,11).

3c-ALEX can monitor multiple distance changes within single molecules

To test whether 3c-ALEX can monitor conformational changes within single molecules by observing three intramolecular distances simultaneously, we compared three triply labeled species having different intramolecular distances (*C3-a*, *C3-b*, and *C3-c* (Fig. 5 *A*)). After sorting and selecting the triply labeled species using the *S* histograms, we obtained three one-dimensional *E** histograms that report on three intramolecular distances (Fig. 5 *B*). In *C3-a* (Fig. 5 *A*, *upper*), in which the three probes are close to one another, significant FRET occurs between all FRET pairs (proximity ratios E^*_{BG}, E^*_{GR}, and E^*_{BR} of 0.42, 0.27, and 0.63, respectively.)

To mimic a conformational change, we shifted the *G* probe by 7 bp toward the 5′-end in *C3-b* (Fig. 5 *A*, *middle*); this increased both the *B-G* distance and the *G-R* distance by ~20 Å compared to the corresponding distances in *C3-a*, but did not change the *B-R* distance. Our results reflect these distance changes: the one-dimensional *E** histograms of *C3-b* (Fig. 5 *B*, *middle*) show decreased FRET between *B* and *G* and also between *G* and *R* (with E^*_{BG} decreasing from 0.42 to 0.13, and E^*_{GR} from 0.27 to 0.10), but no change in the FRET between *B* and *R* (E^*_{BR} remains constant.)

In the same manner, we shifted the *R* probe by 7 bp toward the 3′ end in *C3-c* (Fig. 5 *A*, *lower*), which increased both the *B-R* and *G-R* distances by ~20 Å compared to the corresponding distances in *C3-a*, but did not change the *B-G* distance. Again, our results agree with these distance changes: the one-dimensional *E** histograms of *C3-c* (Fig. 5 *B*, *lower*) show that FRET increases between *B* and *R* and also between *G* and *R*, but not between *B* and *G*. Our results verify that 3c-ALEX can monitor three distances (and thus, three distance changes) simultaneously at the single-molecule level, without auxiliary experiments. This capability can help identify the mobile parts of biomachinery and examine the nature, sequence, and kinetics of conformational changes in biomachines (11,30).

Accurate FRET measurements using 3c-ALEX

Recently, we showed that 2c-ALEX measures FRET accurately by achieving full cross-talk and γ (detection-factor (31)) corrections (24). To examine the ability of 3c-ALEX for accurate FRET measurements, we performed cross-talk and detection-factor corrections for five DNA fragments. Cross-talk and detection-correction factors were obtained from singly and doubly labeled species, respectively (Supplementary Material, Theory of 3c-ALEX and γ-determination). Although each labeled DNA represented a different type of 3c-FRET (Fig. 1 *A*) and a different set of FRET efficiencies, the measured interprobe distances (Fig. 6, *black*; detailed E^*_{XY} and E_{XY} are summarized in Supplementary Material, Table S2) were essentially identical (within 3 Å) and independent of the relative arrangement of the probes. For example, the *B-G* distance in *C2* and *C3-b* was measured to be 88 Å and 85 Å, respectively, and the *B-R* distance in *C2* and *C3-c*, 69 Å and 67 Å, respectively.

Next, we compared distances obtained using 3c-ALEX with identical distances obtained using 2c-ALEX. Since one doubly labeled species provides one distance, individual measurements were taken for *B-G*, *G-R*, and *B-R* (Fig. 6, *gray*). The distances obtained from 3c-ALEX of the triply labeled species are essentially identical (within 3 Å) to those obtained from 2c-ALEX of the doubly labeled species in all cases of measurable FRET ($E > 0.02$). We conclude that, in all cases, 3c-ALEX measures FRET with accuracy similar to that of 2c-ALEX (24). This capability will be useful in using ALEX-based sets of distances to construct models for the structure of large, multi-component complexes (2,28).

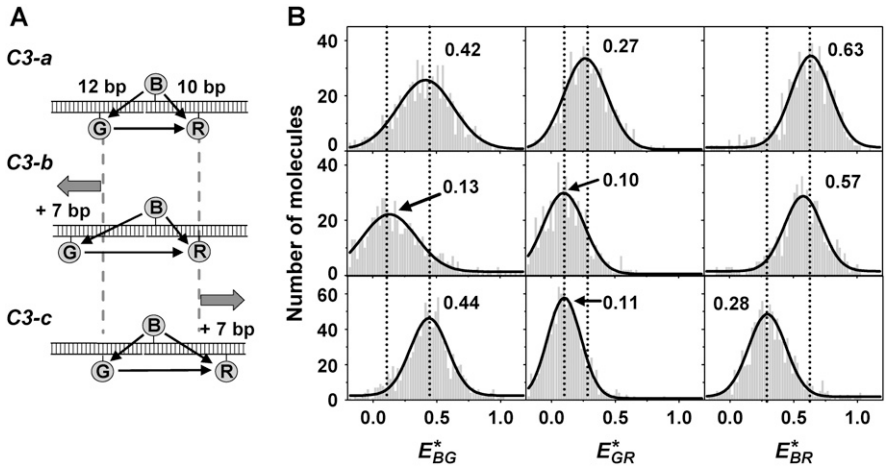

FIGURE 5 Simultaneous observation of three interprobe distances within DNA using 3c-ALEX. (*A*) Labeling scheme (for detail, see Fig. 2). (*B*) One-dimensional *E** histograms of each triply labeled DNA. For both *C3-b* and *C3-c*, moving one probe by seven base pairs relative to its position in *C3-a* DNA results in large changes of two of three proximity ratios; the third proximity ratio is unchanged.

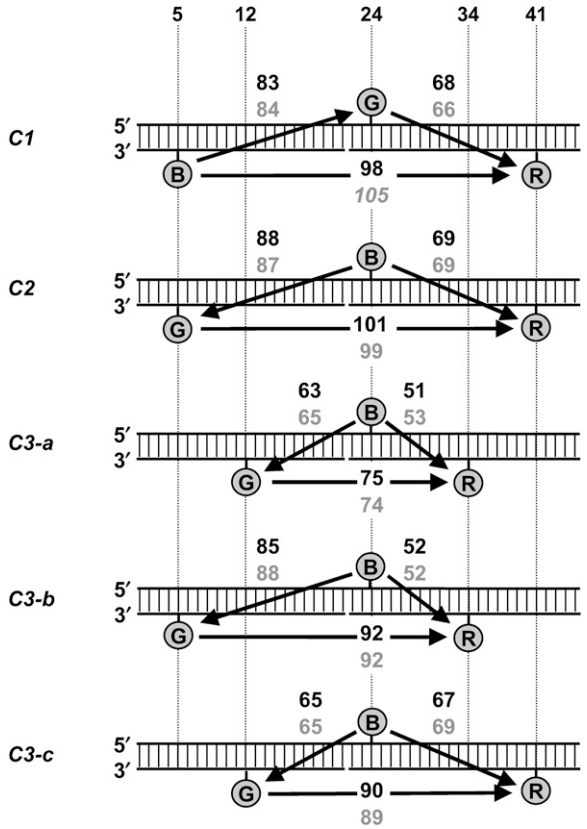

FIGURE 6 Agreement between distances measured using 3c- and 2c-ALEX. Distances (in Å) are next to interprobe arrows. Distances based on 3c- and 2c-ALEX are in black and gray, respectively. Each distance is the average of at least four independent measurements. The standard deviations of distance were ~2 Å with distances <90 Å, and ~4–6 Å with distances ≥90 Å.

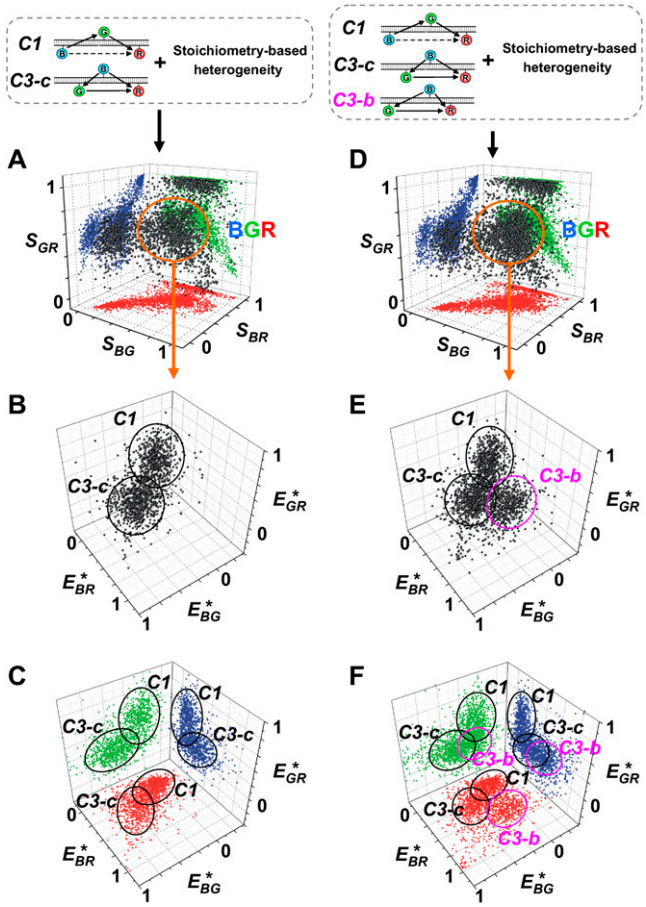

FIGURE 7 Molecule sorting based on both *S* and *E**. (*A*) *S* histogram of a 1:1 mixture of *C1* and *C3-c*, where triply labeled molecules are selected (*orange circle*). (*B*) Three-dimensional *E** histograms of triply labeled species from panel *A*. (*C*) Projections onto three two-dimensional planes of the three-dimensional histogram in *B*. (*D–F*) The same as in *A–C*, respectively, but for a 1:1:1 mixture of *C1*, *C3-c*, and *C3-b*. Note the clear presence of *C3-b* in both the three-dimensional *E** histogram and its projections. The perspectives of *E** histograms are changed compared to those of Fig. 4 *B* to demonstrate clearly the resolution of the three species in three-dimensional space.

Mixture of triply labeled species

In addition to its ability to sort and select molecules based on probe stoichiometry (stoichiometry-based heterogeneity (Fig. 1 *B*)), 3c-ALEX can sort molecules based on FRET; e.g., it can sort triply labeled species based on their structure (conformational heterogeneity (Fig. 1 *B*)). To investigate the ability of 3c-ALEX to observe conformational heterogeneity, we studied an equimolar mixture containing triply labeled species (Fig. 7, *A–C*, *C1* and *C3-c*). After selecting all triply labeled species using the *S* histogram (Fig. 7 *A*), we plotted the selected species on *E** histogram (Fig. 7 *B* for a three-dimensional plot and Fig. 7 *C* for its projections), where two distinct species emerged. The clear separation of these species in the *E** histogram allows graphical selection, *E** measurement, and molecular counting. The measured proximity ratios for Fig. 7 *B* agreed well with those measured from solutions containing a single triply labeled species (data not shown), and the ratio of molecules agrees with the initial mixing ratio (575:646 for *C1*/*C3-c*).

To this mixture, we added another triply labeled species, *C3-b* (Fig. 7, *D–F*). Again, after plotting all triply labeled species in the *E** histogram (Fig. 7, *E* and *F*), we identified three distinct species. Since the three triply labeled species were well separated in the *E** histogram, we selected each species graphically and measured the proximity ratios of all three species. The results agreed well with measurements from single triply labeled species (data not shown); the ratio of molecules agreed with the initial mixing ratio (1.0:1.0:1.2 for *C1*, *C3-b*, and *C3-c*, respectively). We conclude that 3c-ALEX can address structural heterogeneity and report on the structure and relative abundance of each species in solution; in fact, three-dimensional *E** histograms resolve structural heterogeneity better than do the one-dimensional *E** histograms (Supplementary Material, Fig. S3). The enhanced resolution will benefit studies of structural heterogeneity of biomolecules (32–34), and complex processes such as protein and RNA folding (5,6,35,36).

Multi-perspective monitoring of protein translocation on DNA

To demonstrate that 3c-ALEX can monitor multiple conformational changes within large complexes, we monitored the translocation of *Escherichia coli* RNAP on DNA; this translocation occurs when RNAP breaks its initial interactions with DNA (formed in RNAP-promoter open complex, RP_o) and forms an elongation complex (RD_e). Previously, we monitored RNAP translocation on DNA by monitoring a single distance within RP_o and RD_e using the strategies of leading-edge and trailing-edge FRET, both in ensemble (26) and single-molecule experiments (29,37). In leading-edge FRET, forward (i.e., downstream) translocation of RNAP on DNA increases FRET between a donor at the leading edge of RNAP and an acceptor on downstream DNA. In contrast, in trailing-edge FRET, forward translocation of RNAP on DNA decreases FRET between a donor at the trailing edge of RNAP and an acceptor on upstream DNA.

Since 3c-ALEX can report three intramolecular distances simultaneously, we reasoned that we can merge leading- and trailing-edge FRET in a 3c-ALEX assay that monitors simultaneously two protein-DNA and one DNA-DNA distances (Fig. 8 *A*) in a single RNAP-DNA complex. By incorporating a *G* probe on RNAP, a *B* probe on upstream DNA, and an *R* probe on downstream DNA, RNAP translocation downstream is expected to decrease the $B \rightarrow G$ FRET (equivalent to trailing-edge FRET), and concurrently increase the $G \rightarrow R$ FRET (equivalent to leading-edge FRET); the $B \rightarrow R$ FRET may or may not change. Therefore, we prepared a singly labeled RNAP by attaching a *G* probe to position 496 of σ^{70} (26,28,38), and a doubly labeled promoter DNA fragment with a *B* and *R* probe at its upstream and downstream ends, respectively (Fig. 8 *A*). Residue 496 on σ^{70} was chosen based on its location on structural models of the open complex (28,39); incorporation of a *G* probe on residue 496 was expected to yield measurable FRET efficiencies for both trailing- and leading-edge FRET (in a triply labeled open complex), and yield significant and opposite-sign FRET changes upon downstream RNAP translocation. We then formed RP_o (Fig. 8 *A*, *upper*) and elongation complex $RD_{e,12}$ (26), where RNAP has translocated downstream by a full turn of DNA relative to its position in RP_o (Fig. 8 *A*), and performed 3c-ALEX.

The *S* histograms for RP_o and $RD_{e,12}$ (not shown) were similar, confirming that σ^{70} is not released during the transition of RNAP to elongation (26,29). A substantial release of σ^{70} would have converted one triply labeled molecule (RP_o, a *B-G-R* species) into one singly labeled molecule (free σ^{70}, a *G*-only species) and one doubly labeled molecule (free DNA, a *B-R* species), changing the *S* histogram substantially. Moreover, a comparison of E^* histograms for triply labeled RP_o and $RD_{e,12}$ showed that for ~85% of the complexes, trailing-edge FRET decreases substantially (mean E^*_{BG} decreases from 0.51 to 0.10; Fig. 8 *B*, *left*), whereas leading-edge FRET increases substantially (mean E^*_{GR} increases from 0.03 to 0.32; Fig. 8 *B*, *middle*). These FRET changes correspond to an overall downstream translocation of RNAP on DNA, which increases the distance within the trailing-edge FRET probe pair and decreases the distance within the leading-edge FRET probe pair. This way, the direction of RNAP movement is unequivocally determined with a single measurement. Our results should promote real-time analysis of the conformational changes during transcription and other nucleic-acid processing pathways.

CONCLUSION AND OUTLOOK

Using DNA and transcription complexes, we showed that 3c-ALEX is an excellent tool for extracting multiple stoichiometries and multiple distances within single fluorescent molecules, independent of the extent of FRET among the probes used. We also established that 3c-ALEX allows accurate FRET measurements among multiple FRET pairs, and that both probe stoichiometry and FRET efficiency can be used to sort, identify, select, and further analyze species in complex mixtures. 3c-ALEX is well-suited for analyzing complex biological processes, such as assembly or disassembly of multi-component complexes (30), protein and

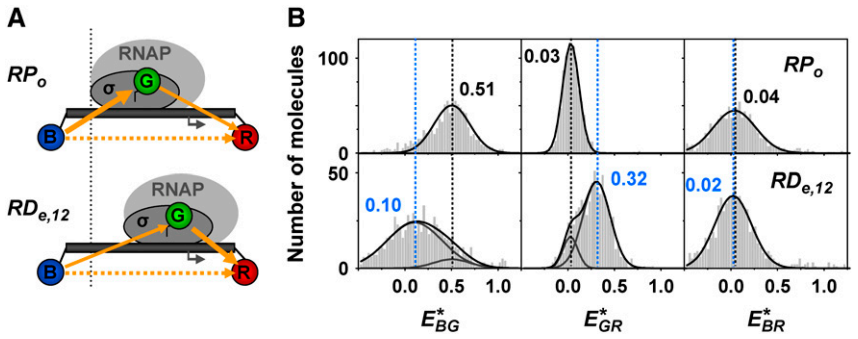

FIGURE 8 Multi-perspective monitoring of a protein translocation on DNA. (*A*) Concept and labeling scheme. Triply labeled transcription complexes are prepared; the *G* probe (Cy3B) is on RNAP and the *B* (Alexa 488) and *R* (Alexa 647) probes upstream and downstream of the RNAP binding site, respectively. $B \rightarrow G$, trailing-edge FRET pair; $G \rightarrow R$, leading-edge FRET pair. The direction of transcription (and of downstream translocation) is denoted by the black arrow on DNA. Upon RNAP translocation downstream, trailing-edge FRET decreases and, correspondingly, leading-edge FRET increases, reporting on the direction of motion. (*B*) Comparison of one-dimensional proximity-ratio histograms for RP_o and $RD_{e,12}$ show that for ~85% of the complexes, trailing-edge FRET decreases (as measured by E^*_{BG}) and leading-edge FRET correspondingly increases (as measured by E^*_{GR}), consistent with downstream RNAP translocation. The remaining 15% of the complexes are inactive (29).

RNA folding, and multi-step signal-transduction cascades. 3c-ALEX can also aid in ultrasensitive protein-ligand binding assays (40), biosensing (8), and multiplexing (41).

To measure real-time dynamics and reaction trajectories of many individual molecules simultaneously, 3c-ALEX can be extended to immobilized molecules, using either total internal reflection (37,42) or confocal microscopy. Studies of immobilized molecules by 3c-ALEX will directly report on the nature, sequence, coupling, and kinetics of conformational changes occurring during biological mechanisms, providing detailed views of molecular machines at work.

3c-ALEX can also be realized by using three interlaced pulsed-lasers (36,43), which will add fluorescence lifetime information to the current observables and be useful for cross-talk-free multi-color fluorescence imaging microscopy and fluorescence cross-correlation spectroscopy.

Multi-distance analysis by 3c-ALEX is the first step toward n-color-ALEX which, in principle, should enable observation of n-component interactions and determination of up to $(n(n-1)/2)$ distances within single molecules. The collection of multiple distances (through simple triangulation) will unequivocally determine the probe positions in three-dimensional space, and provide restraints for constructing low-resolution, solution-based structures of large, multi-component complexes intractable due to excessive heterogeneity, limited quantity, or transient nature.

SUPPLEMENTARY MATERIAL

An online supplement to this article can be found by visiting BJ Online at http://www.biophysj.org.

We thank Dr. C. Meares (University of California, Davis) for plasmid pGEMD496C, Sangjin Kim for helping with the initial work, and J. Tang for editorial assistance.

This work was funded by a National Research Laboratory grant and a Chemical Genomics grant of the Korean Science and Engineering Foundation and Ministry of Science and Technology to S.K.K., and National Institutes of Health grant GM65382 and GM069709-01A1 and Department of Energy grants FG03-02ER6339 and 04ER63938 to S.W.

REFERENCES

1. Selvin, P. R. 2000. The renaissance of fluorescence resonance energy transfer. *Nat. Struct. Biol.* 7:730–734.
2. Heyduk, T. 2002. Measuring protein conformational changes by FRET/LRET. *Curr. Opin. Biotechnol.* 13:292–296.
3. Clegg, R. M. 1992. Fluorescence resonance energy transfer and nucleic acids. *Methods Enzymol.* 211:353–388.
4. Weiss, S. 1999. Fluorescence spectroscopy of single biomolecules. *Science.* 283:1676–1683.
5. Zhuang, X. W., and M. Rief. 2003. Single-molecule folding. *Curr. Opin. Struct. Biol.* 13:88–97.
6. Ha, T. 2004. Structural dynamics and processing of nucleic acids revealed by single-molecule spectroscopy. *Biochemistry.* 43:4055–4063.
7. Horsey, I., W. S. Furey, J. G. Harrison, M. A. Osborne, and S. Balasubramanian. 2000. Double fluorescence resonance energy transfer to explore multicomponent binding interactions: a case study of DNA mismatches. *Chem. Commun.*1043–1044.
8. Medintz, I. L., A. R. Clapp, H. Mattoussi, E. R. Goldman, B. Fisher, and J. M. Mauro. 2003. Self-assembled nanoscale biosensors based on quantum dot FRET donors. *Nat. Mater.* 2:630–638.
9. Galperin, E., V. Verkhusha, and A. Sorkin. 2004. Three-chromophore FRET microscopy to analyze multiprotein interactions in living cells. *Nat. Methods.* 1:209–217.
10. Ramirez-Carrozzi, V. R., and T. K. Kerppola. 2001. Dynamics of Fos-Jun-NFAT1 complexes. *Proc. Natl. Acad. Sci. USA.* 98:4893–4898.
11. Klostermeier, D., P. Sears, C. H. Wong, D. P. Millar, and J. R. Williamson. 2004. A three-fluorophore FRET assay for high-throughput screening of small-molecule inhibitors of ribosome assembly. *Nucleic Acids Res.* 32:2707–2715.
12. Watrob, H. M., C. P. Pan, and M. D. Barkley. 2003. Two-step FRET as a structural tool. *J. Am. Chem. Soc.* 125:7336–7343.
13. Liu, J. W., and Y. Lu. 2002. FRET study of a trifluorophom-labeled DNAzyme. *J. Am. Chem. Soc.* 124:15208–15216.
14. Heilemann, M., P. Tinnefeld, G. S. Mosteiro, M. G. Parajo, N. F. Van Hulst, and M. Sauer. 2004. Multistep energy transfer in single molecular photonic wires. *J. Am. Chem. Soc.* 126:6514–6515.
15. Haustein, E., M. Jahnz, and P. Schwille. 2003. Triple FRET: a tool for studying long-range molecular interactions. *ChemPhysChem.* 4:745–748.
16. Vyawahare, S., S. Eyal, K. D. Mathews, and S. R. Quake. 2004. Nanometer-scale fluorescence resonance optical waveguides. *Nano Lett.* 4:1035–1039.
17. Serin, J. M., D. W. Brousmiche, and J. M. J. Frechet. 2002. Cascade energy transfer in a conformationally mobile multichromophoric dendrimer. *Chem. Commun.*2605–2607.
18. Tong, A. K., S. Jockusch, Z. M. Li, H. R. Zhu, D. L. Akins, N. J. Turro, and J. Y. Ju. 2001. Triple fluorescence energy transfer in covalently trichromophore-labeled DNA. *J. Am. Chem. Soc.* 123:12923–12924.
19. Hohng, S., C. Joo, and T. Ha. 2004. Single-molecule three-color FRET. *Biophys. J.* 87:1328–1337.
20. Clamme, J. P., and A. A. Deniz. 2005. Three-color single-molecule fluorescence resonance energy transfer. *ChemPhysChem.* 6:74–77.
21. Heinze, K. G., M. Jahnz, and P. Schwille. 2004. Triple-color coincidence analysis: one step further in following higher order molecular complex formation. *Biophys. J.* 86:506–516.
22. Deniz, A. A., M. Dahan, J. R. Grunwell, T. Ha, A. E. Faulhaber, D. S. Chemla, S. Weiss, and P. G. Schultz. 1999. Single-pair fluorescence resonance energy transfer on freely diffusing molecules: observation of Forster distance dependence and subpopulations. *Proc. Natl. Acad. Sci. USA.* 96:3670–3675.
23. Kapanidis, A. N., N. K. Lee, T. A. Laurence, S. Doose, E. Margeat, and S. Weiss. 2004. Fluorescence-aided molecule sorting: analysis of structure and interactions by alternating-laser excitation of single molecules. *Proc. Natl. Acad. Sci. USA.* 101:8936–8941.
24. Lee, N. K., A. N. Kapanidis, Y. Wang, X. Michalet, J. Mukhopadhyay, R. H. Ebright, and S. Weiss. 2005. Accurate FRET measurements within single diffusing biomolecules using alternating-laser excitation. *Biophys. J.* 88:2939–2953.
25. Kapanidis, A. N., T. A. Laurence, N. K. Lee, E. Margeat, X. Kong, and S. Weiss. 2005. Alternating-laser excitation of single molecules. *Acc. Chem. Res.* 38:523–533.
26. Mukhopadhyay, J., A. N. Kapanidis, V. Mekler, E. Kortkhonjia, Y. W. Ebright, and R. H. Ebright. 2001. Translocation of $\sigma(70)$ with RNA polymerase during transcription: Fluorescence resonance energy transfer assay for movement relative to DNA. *Cell.* 106:453–463.
27. Callaci, S., and T. Heyduk. 1998. Conformation and DNA binding properties of a single-stranded DNA binding region of $\sigma(70)$ subunit from *Escherichia coli* RNA polymerase are modulated by an interaction with the core enzyme. *Biochemistry.* 37:3312–3320.
28. Mekler, V., E. Kortkhonjia, J. Mukhopadhyay, J. Knight, A. Revyakin, A. N. Kapanidis, W. Niu, Y. W. Ebright, R. Levy, and R. H. Ebright. 2002. Structural organization of bacterial RNA polymerase holoenzyme and the RNA polymerase-promoter open complex. *Cell.* 108:599–614.

29. Kapanidis, A. N., E. Margeat, T. A. Laurence, S. Doose, S. O. Ho, J. Mukhopadhyay, E. Kortkhonjia, V. Mekler, R. H. Ebright, and S. Weiss. 2005. Retention of transcription initiation factor σ70 in transcription elongation: single-molecule analysis. *Mol. Cell.* 20: 347–356.

30. Blanchard, S. C., H. D. Kim, R. L. Gonzalez, J. D. Puglisi, and S. Chu. 2004. tRNA dynamics on the ribosome during translation. *Proc. Natl. Acad. Sci. USA.* 101:12893–12898.

31. Ha, T. J., A. Y. Ting, J. Liang, W. B. Caldwell, A. A. Deniz, D. S. Chemla, P. G. Schultz, and S. Weiss. 1999. Single-molecule fluorescence spectroscopy of enzyme conformational dynamics and cleavage mechanism. *Proc. Natl. Acad. Sci. USA.* 96:893–898.

32. Rothwell, P. J., S. Berger, O. Kensch, S. Felekyan, M. Antonik, B. M. Wohrl, T. Restle, R. S. Goody, and C. A. M. Seidel. 2003. Multiparameter single-molecule fluorescence spectroscopy reveals heterogeneity of HIV-1 reverse transcriptase: primer/template complexes. *Proc. Natl. Acad. Sci. USA.* 100:1655–1660.

33. Ying, L. M., J. J. Green, H. T. Li, D. Klenerman, and S. Balasubramanian. 2003. Studies on the structure and dynamics of the human telomeric G quadruplex by single-molecule fluorescence resonance energy transfer. *Proc. Natl. Acad. Sci. USA.* 100:14629–14634.

34. Yang, H., G. B. Luo, P. Karnchanaphanurach, T. M. Louie, I. Rech, S. Cova, L. Y. Xun, and X. S. Xie. 2003. Protein conformational dynamics probed by single-molecule electron transfer. *Science.* 302: 262–266.

35. Talaga, D. S., W. L. Lau, H. Roder, J. Y. Tang, Y. W. Jia, W. F. DeGrado, and R. M. Hochstrasser. 2000. Dynamics and folding of single two-stranded coiled-coil peptides studied by fluorescent energy transfer confocal microscopy. *Proc. Natl. Acad. Sci. USA.* 97:13021–13026.

36. Laurence, T. A., X. X. Kong, M. Jager, and S. Weiss. 2005. Probing structural heterogeneities and fluctuations of nucleic acids and denatured proteins. *Proc. Natl. Acad. Sci. USA.* 102:17348–17353.

37. Margeat, E., A. N. Kapanidis, P. Tinnefeld, Y. Wang, J. Mukhopadhyay, R. H. Ebright, and S. Weiss. 2006. Direct observation of abortive initiation and promoter escape within single immobilized transcription complexes. *Biophys. J.* 90:1419–1431.

38. Nickels, B. E., J. Mukhopadhyay, S. J. Garrity, R. H. Ebright, and A. Hochschild. 2004. The sigma 70 subunit of RNA polymerase mediates a promoter-proximal pause at the lac promoter. *Nat. Struct. Mol. Biol.* 11:544–550.

39. Lawson, C. L., D. Swigon, K. S. Murakami, S. A. Darst, H. M. Berman, and R. H. Ebright. 2004. Catabolite activator protein: DNA binding and transcription activation. *Curr. Opin. Struct. Biol.* 14:10–20.

40. Mayer, T. U. 2003. Chemical genetics: tailoring tools for cell biology. *Trends Cell Biol.* 13:270–277.

41. Tong, A. K., Z. M. Li, G. S. Jones, J. J. Russo, and J. Y. Ju. 2001. Combinatorial fluorescence energy transfer tags for multiplex biological assays. *Nat. Biotechnol.* 19:756–759.

42. Friedman, L. J., J. Chung, and J. Gelles. 2006. Viewing dynamic assembly of molecular complexes by multi-wavelength single-molecule fluorescence. *Biophys. J.* 91:1023–1031.

43. Muller, B. K., E. Zaychikov, C. Brauchle, and D. C. Lamb. 2005. Pulsed interleaved excitation. *Biophys. J.* 89:3508–3522.